CHAPTER I

INTRODUCTION

1.1 ISOTOPIC FRACTIONATION

The partitioning of isotopes of an element in two or more phases by different physico-chemical processes is called isotopic fractionation. There are two major classes of processes (i) isotopic exchange reactions (equilibrium process) and (ii) kinetic processes (such as diffusion, condensation, evaporation etc.) responsible for the isotopic fractionation in nature. The theoretical basis for estimating the magnitude of fractionation for each of these processes differ, but the underlying principle for each is that the effects are dependent on mass.

The mass-dependent isotopic fractionation obeys a simple rule. For example, for three oxygen isotopes (^{16}O, ^{17}O and ^{18}O) we have,

$$^{17}R_A / {}^{17}R_B = \left({}^{18}R_A / {}^{18}R_B \right)^{\beta} \qquad (1.1)$$

where, $^{17}R_A$ and $^{17}R_B$ are the abundance ratios ^{17}O / ^{16}O and $^{18}R_A$ and $^{18}R_B$ are the abundance ratios ^{18}O / ^{16}O in phases A and B respectively. The exponent β depends on the mass of the isotopes and differs slightly for different processes. It is a common practice to denote the isotopic ratios in δ-notation, where δ (in per mil) is defined by,

$$\delta\,(‰) = \left(\frac{R_{sample}}{R_{std}} - 1 \right) \times 1000 \qquad (1.2)$$

R_{sample} and R_{std} are the isotope ratios (^{17}O / ^{16}O or ^{18}O / ^{16}O) of a sample and a standard material respectively. The non-linear fractionation curve of Eqn. 1.1 can be approximated in δ-notation as a straight line in the three-isotope space with a slope β:

$$\delta\,^{17}O = \beta \left(\delta\,^{18}O \right) \qquad (1.3)$$

A fractionation process can be comprehensively studied if it involves an element with three or more isotopes. The best examples are oxygen (^{16}O, ^{17}O and ^{18}O), sulfur (^{32}S, ^{33}S, ^{34}S, ^{36}S), Mg (^{24}Mg, ^{25}Mg and ^{26}Mg) etc. The calculated β for oxygen is nearly 0.5 (ranging from 0.51 to 0.52 depending upon the particular process involved) (Urey, 1947; Craig, 1957; Matsuhisa et al., 1978; Young et al., 2002). Therefore, for oxygen, Eqn. 1.3 is generally written as,

$$\delta\,^{17}O = 0.52 \left(\delta\,^{18}O \right) \qquad (1.4)$$

Experimentally, the oxygen isotopic composition of most of the terrestrial, lunar and some meteoritic materials lie on a line with a slope (~ 0.5) in a three-isotope plot as shown in Figure 1.1.

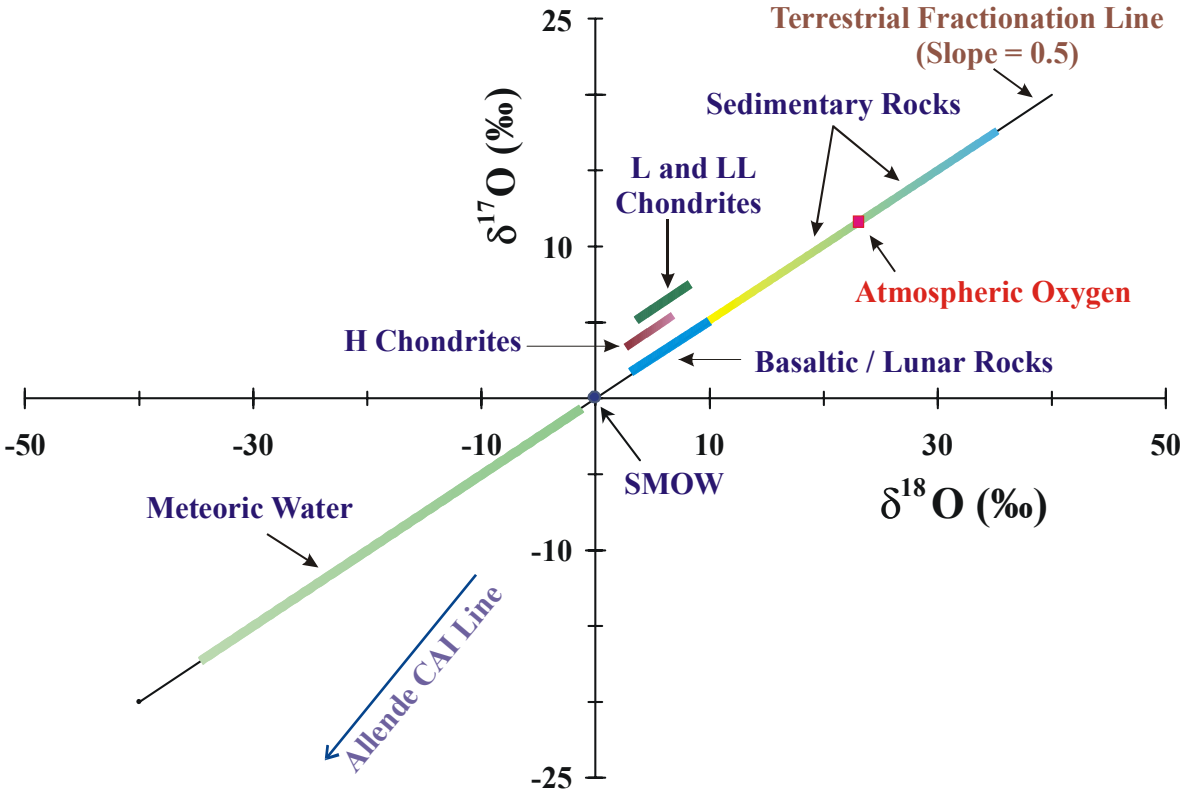

Figure 1.1. *Three-isotope plot of the oxygen isotopic compositions of various terrestrial materials, which define a mass dependent fractionation line known as terrestrial mass fractionation line. Along with the Allende CAI line, the compositions of three classes of chondritic meteorites (L, LL and H) and the Lunar rocks are shown in the diagram. SMOW represents standard mean ocean water, a reference for all oxygen isotopic measurements.*

1.1.1 Mass Independent Isotopic Fractionation

Though rare, there are processes in nature, which do not follow the above mass-dependent fractionation rule. These processes display mass independent or non-mass dependent isotopic fractionation. For oxygen isotopes, the mass independent fractionation is readily apparent when,

$$\delta^{17}O \neq 0.52\left(\delta^{18}O\right) \qquad (1.5)$$

And the degree of mass independent fractionation is denoted by

$$\Delta^{17}O = \delta^{17}O - 0.52\left(\delta^{18}O\right) \qquad (1.6)$$

There are two natural systems where mass independent isotopic fractionations have been observed are described below.

1.1.2 The Early Solar System

The first mass independent oxygen isotopic anomaly was discovered in CAIs (calcium-aluminium rich inclusion) in Allende meteorite (Clayton et al., 1973) and was used as an indicator for nucleosynthetic anomaly. The ^{16}O enrichment in these refractory objects was explained by invoking addition of nearly pure ^{16}O component to the proto-solar cloud from a nearby supernova (Clayton et al., 1973). After more than 25 years of measurements, meteoritic oxygen isotope anomalies have not been observed to correlate with anomalies of any other isotopes such as silicon or magnesium (Thiemens, 1999). Moreover, oxygen isotopic investigations of individual pre-solar grains have not detected any evidence for ^{16}O carriers (Hutcheon et al., 1994; Huss et al., 1994). In fact, corundum grains from Bishunpur (Huss et al., 1994) and Orgueil (Hutcheon et al., 1994) show large ^{17}O enrichment. Nittler et al. (1994) have reported 21 interstellar oxide grains (Al_2O_3) from the Tieschitz meteorite and concluded that they have not found any grain with large ^{16}O enrichment, which would be consistent with the notion of a ^{16}O carrier. Thus, "while there is unmistakable evidence for interstellar grains carrying anomalous oxygen, their oxygen isotopic composition does not support the notion of admixture of pure ^{16}O component" (Thiemens, 1996). Therefore, the process responsible for the generation of these isotopic compositions is still not clear and more study is required to put constraints on various models.

1.1.3 Earth and Other Planetary Atmosphere

Stratospheric ozone is found to be enriched in both the heavy oxygen isotopes ^{18}O and ^{17}O and the enrichment is predominantly mass independent (Mauersberger, 1981, 1987; Mauersberger et al., 2001; Schueler et al., 1990; Krankowsky et al., 2000). Mass independent isotopic compositions were also found in a number of atmospheric species, such as stratospheric and mesospheric CO_2, atmospheric CO and N_2O (Thiemens et al., 1991, 1995; Rahn and Wahlen, 1997; Yung and Miller, 1997; Cliff and Thiemens, 1997; Huff and Thiemens, 1998; Röckmann et al., 1998; Weston, 1999).

Mass independent oxygen isotopic composition is not limited to the Earth's atmosphere, but is also found in the water extracted from hydrated minerals and CO_2 extracted from carbonates of SNC group of Martian meteorites (Karlsson et al., 1992; Farquhar et al., 1998)

1.1.4 Laboratory Observations

It was shown by a novel laboratory experiment (Thiemens and Heidenreich, 1983) that chemical processes could generate mass independent isotopic fractionation. Ozone formed from molecular oxygen by electric discharge has extremely enriched heavy oxygen isotopes and surprisingly has $\delta^{17}O = \delta^{18}O$ instead of $\delta^{17}O \sim 0.5\ \delta^{18}O$. Subsequently the potential of the photochemical /chemical processes in generating mass independent isotopic fractionation has been shown in various laboratory studies ($O + CO \rightarrow CO_2$; $SF_5 + SF_5 \rightarrow S_2F_{10}$; isotopic exchange $O(^1D) + CO_2 \rightarrow O(^3P) + CO_2$; $OH + CO \rightarrow CO_2 + H$) (Bhattacharya and Thiemens, 1989; Bains and Thiemens, 1989; Wen and Thiemens, 1993; Röckmann et al., 1998; Johnston et al., 2000).

Based on these laboratory experiments, it was argued that certain photochemical/ chemical processes have the potential to explain the mass independent isotopic fractionations observed in the atmosphere. Similar kind of photo-induced chemical processes can be invoked in a nebular environment to explain the isotopic anomaly observed in early solar system solids (Thiemens, 1999).

1.1.5 Accurate Expressions of Isotopic Fractionation

Equations 1.3 through 1.6 are the simplified approximation of equation 1.1. Recently, in few publications (Miller, 2002 and reference therein) these relations are presented in accurate form, showing non-linearity in a three-isotope plot between $\delta^{18}O$ and $\delta^{17}O$ for the cases where the sample data set includes points with greater $|\delta^{17}O|$ and $|\delta^{18}O|$. These non-linear expressions may be important for interpreting the data set, where the isotopic compositions marginally deviate from the terrestrial silicate composition (as for example, atmospheric oxygen). Moreover, in the case of oxygen from extraterrestrial reservoirs, where mass dependent fractionation line may be off-set parallel to that of the bulk silicate Earth, an extra term is necessary in equation 1.1 to quantify the off-set (Miller, 2002). Depending on these advancements, high precision data sets reported on the basis of $\delta^{18}O$ versus $\delta^{17}O$ plot need to be reassessed. However, the study presented in this thesis does not use directly any of these relationships to interpret the data, therefore, are not elaborated here.

1.2 OBJECTIVE OF THE PRESENT STUDY

The objective of this thesis is to explore the basic processes of mass independent fractionation based on laboratory investigation of oxygen isotopic fractionation in some photochemical/ chemical processes.

To study the mass independent fractionation process in the laboratory, ozone is an attractive molecule since large mass independently fractionated ozone can be easily generated in the laboratory. Moreover, in the stratosphere, ozone is mass independently enriched in heavy oxygen isotopes (as mentioned earlier) and controls the oxygen isotopic distribution among other oxygen containing stratospheric trace species. Therefore, some results of the laboratory-based investigations related to ozone can be directly applied to the stratosphere for better understanding of the stratospheric isotope chemistry.

There are number of laboratory studies related to mass independent oxygen isotopic fractionation in ozone (Thiemens and Jackson, 1987, 1988; Morton et al., 1990; Wen and Thiemens, 1991; Mauersberger et al., 1999). Still there are several basic questions unanswered regarding origin of mass independent isotopic anomaly during ozone formation and dissociation. In addition, there are unsettled issues pertaining to stratospheric ozone isotopic anomaly and transfer of oxygen isotopic anomaly from ozone to other stratospheric molecules.

A number of laboratory experiments were devised in the present study to cover these aspects. The specific studies undertaken are:

(i) Investigation of pressure dependence of heavy oxygen isotope enrichment in ozone in the pressure range 600 to 8 torr with a fine resolution.

(ii) Investigation of isotope enrichment variation in ozone with the amount of ozone produced.

(iii) Isotopic effect in photo-dissociation of ozone in Hartley and Chappuis band.

(iv) Isotopic effect during ozone dissociation by interaction with a surface.

(v) Isotopic fractionation during $O(^1D) - CO_2$ isotopic exchange reaction.

A schematic representation of the present study, showing the objective and specific investigations, is shown in Figure 1.2

In the following section, a brief summary of the various aspects relevant to our understanding of the origin of mass independent fractionation in ozone and a summary of stratospheric observations are presented.

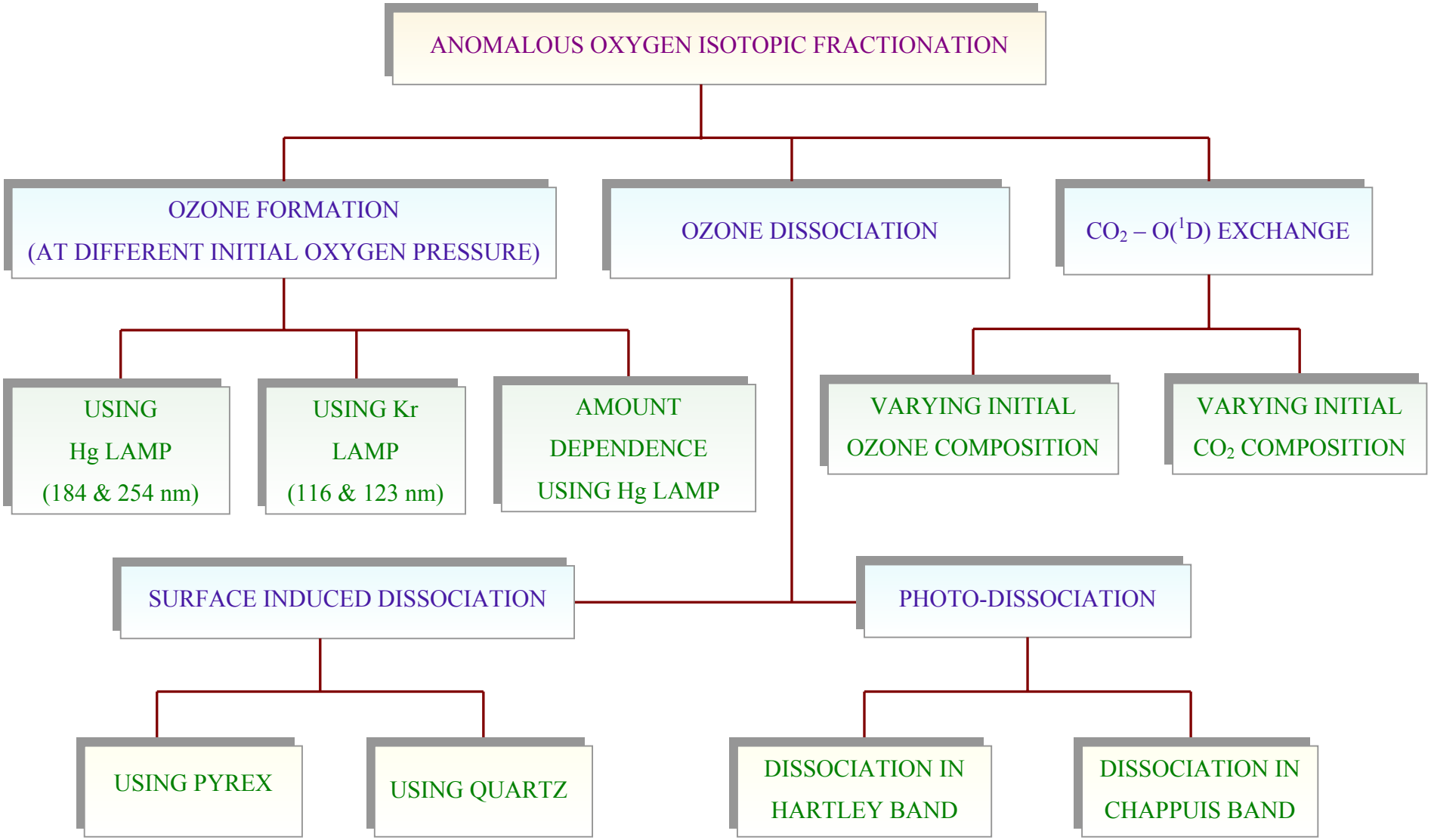

Figure 1.2. *A schematic representation of the present study showing the objective and specific investigations carried out.*

1.3 OZONE FORMATION MECHANISM

According to Chapman mechanism, ozone is formed through the photolysis of oxygen below 185 nm followed by third body recombination of ground state O-atoms with O_2 molecules to form O_3.

$$O_2 + h\nu \rightarrow O + O \ (\lambda < 185 \text{ nm}) \qquad (1.7)$$

$$O + O_2 + M \rightarrow O_3 + M \qquad (1.8)$$

The photo-dissociation coefficient of eqn. 1.7 is 1.2×10^{-12} /sec in Earth's atmosphere at 25 km and the rate coefficient of eqn. 1.8 is 6×10^{-34} cm^6 mol^{-2} sec^{-1} (at 300 K). Ozone so formed is dissociated by visible and UV wavelengths and by O-atoms,

$$O_3 + h\nu \rightarrow O_2 + O \qquad (1.9)$$

$$O + O_3 \rightarrow 2O_2 \qquad (1.10)$$

The photo-dissociation coefficient of eqn. 1.9 is 2.1×10^{-4} /sec in Earth's atmosphere at 25 km and the rate coefficient of eqn. 1.10 is 8×10^{-15} cm^3 mol^{-1} sec^{-1} (at 298 K). The photo-dissociation coefficients and rate constants are from DeMore et al. (1997). The cycle is shown pictorially in Figure 1.3.

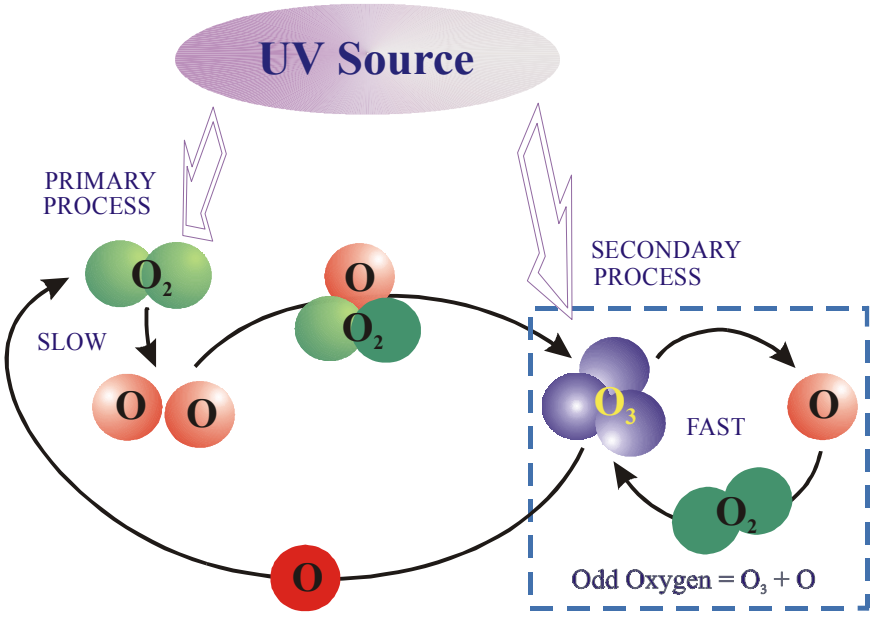

Figure 1.3. *Schematic reaction scheme of ozone formation by oxygen photolysis. The primary and secondary processes are shown separately. The conversion between O_3 and O is fast (relative to the primary process) and together they are called the odd oxygen.*

1.3.1 Isotopic Enrichment in Ozone

The formation of ozone in the laboratory is always associated with heavy oxygen isotopic enrichment (mass independent) relative to the initial oxygen composition. The enrichment is almost equal in both ^{17}O and ^{18}O. The relative enrichment is more (about 100 ‰) when ozone is formed by the above mentioned reaction chain (Thiemens and Jackson, 1987, 1988) compared to the formation by electric discharge in molecular oxygen (Thiemens and Heidenreich, 1983). The latter results in an enrichment of about 30 ‰.

To explain this heavy isotopic enrichment, Heidenreich and Thiemens (1986) suggested a symmetry-selective process in the formation reaction. For ozone species $^{49}O_3$ and $^{50}O_3$, about one-third of all the molecules are symmetric (for example, $^{16}O^{18}O^{16}O$), and two-thirds are asymmetric (for example, $^{16}O^{16}O^{18}O$). It was proposed that the asymmetric reaction intermediate in the $O + O_2$ collision has a longer lifetime than the symmetric reaction intermediate, which results in an efficient quenching to ground state ozone (Heidenreich and Thiemens, 1986).

The apparent role of symmetry was found during the measurements of the distribution of all ozone isotopomers. A slight depletion of heavy symmetric isotopomers $^{17}O^{17}O^{17}O$ and $^{18}O^{18}O^{18}O$ was observed along with an enrichment (~ 18 %) of the asymmetric combination $^{16}O^{17}O^{18}O$. The enrichment in all other isotopomers was found to be about one-third less compared to that of $^{16}O^{17}O^{18}O$ (Krankowsky and Mauersberger, 1996).

Gellene (1996) proposed a mechanism based on nuclear symmetry to model the above observations. According to this approach, symmetry restriction arises for homonuclear diatomics ($^{16}O^{16}O$ and $^{18}O^{18}O$) involved in the $O + O_2$ collision because a fraction of their rotational states correlate with those of corresponding ozone molecule. On the other hand, for heteronuclear molecules ($^{16}O^{18}O$), all their rotational states correlate with those of the resulting ozone molecule. This model can reproduce the general features of the observation by Krankowsky and Mauersberger (1996), but cannot be satisfactorily applied for the other laboratory studies (Thiemens and Jackson, 1987, 1988; Morton et al., 1990).

1.3.2 Relative Rate Coefficient of Different Ozone Formation Channels

Determination of the rate coefficient of different ozone formation channels (Anderson et al., 1997; Mauersberger et al., 1999; Janssen et al., 1999) clarified the role

of symmetry. The reaction channels 1, 12 and 36 (shown in Table 1.1) show nearly the similar rate whereas the channel 24 shows an advantage of 50 %. The channels 12 and 24 produce mainly asymmetric molecules (colliding atom becoming the end member), $^{18}O^{16}O^{16}O$ and $^{16}O^{18}O^{18}O$ respectively. The difference in the rate coefficients of these two reactions indicates that symmetry plays a complex role in the isotope enrichment process (Anderson et al., 1997).

The reactions 12 and 13 of Table 1.1 are indeed end-on process without forming symmetric molecules whereas the heteronuclear oxygen reactions (reactions 10 and 11) for the same isotopomers ($^{18}O^{16}O^{16}O$ and $^{16}O^{18}O^{16}O$) show a pronounced difference in the formation rates of the symmetric and asymmetric species (1.45 and 1.08 respectively). These two are exclusively responsible for the enrichment in $^{50}O_3$, making an over all rate of 1.27 for the $^{16}O + {}^{16}O^{18}O$ channel (Janssen et al., 1999).

At present the rate constant investigation study is not complete. Specifically, the investigations involving the rare isotope ^{17}O (which make the experiments more challenging) distribution in ozone isotopomers has to be carried out.

1.3.3 Non-RRKM Based Model

In a series of recent publications (Hathorn and Marcus, 1999, 2000; Gao and Marcus, 2001, 2002; Marcus and Gao, 2001), Marcus and his co-workers (at CalTech) developed a model to explain the anomalous oxygen isotopic composition during ozone formation. Their work is based on the statistical theory developed by Rice, Ramsperger, Kassel and Marcus over a long period and known as RRKM theory of unimolecular dissociation/ bimolecular recombination in its vibrational form (Marcus, 1952a, 1952b, 1968). It involves the formation of vibrationally excited ozone isotopomers from the recombination of O and O_2 with a hindered-rotor transition state.

In RRKM theory, for a bimolecular recombination, $X + YZ \rightarrow XYZ^*$ ('*' denoting vibrationally excited molecule), the vibrational-rotational energy is supposed to be statistically distributed among its vibrational-rotational modes. This excited molecule can redissociate, $XYZ^* \rightarrow (X + YZ)$ or $(XY + Z)$ or lose its energy by collision to form a stable XYZ molecule. The unimolecular dissociation rate constant for a vibrationally excited molecule of vibrational-rotational energy E and total angular momentum J is given by,

$$K_{EJ} = N^{+}_{EJ} / h\rho_{EJ} \qquad (1.11)$$

N_{EJ}^{+} is the number of quantum states accessible to the 'transition state' for dissociation for the given E and J and ρ_{EJ} is the density (number per unit energy) of quantum states of the vibrationally excited molecule.

Table 1.1. *Reaction channels of all possible oxygen combinations leading to ozone molecules with the exit channel specific rate coefficient. The rate coefficients are relative to the standard rate for* $^{16}O + {}^{16}O^{18}O + M$ of 6.05×10^{-34} cm^6 sec^{-1} *[Janssen et al., 1999 and the references therein].*

Mass	Reaction channel no.	Reaction	Relative rate coefficient
48	1	$^{16}O + {}^{16}O^{16}O \rightarrow {}^{16}O^{16}O^{16}O$	1.00
49	2	$^{16}O + {}^{16}O^{17}O \rightarrow {}^{16}O^{16}O^{17}O$	
	3	$\rightarrow {}^{16}O^{17}O^{16}O$	
	4	$^{17}O + {}^{16}O^{16}O \rightarrow {}^{17}O^{16}O^{16}O$	1.03
	5	$\rightarrow {}^{16}O^{17}O^{16}O$	
50	6	$^{16}O + {}^{17}O^{17}O \rightarrow {}^{16}O^{17}O^{17}O$	1.23
	7	$\rightarrow {}^{17}O^{16}O^{17}O$	
	8	$^{17}O + {}^{16}O^{17}O \rightarrow {}^{17}O^{16}O^{17}O$	
	9	$\rightarrow {}^{17}O^{17}O^{16}O$	
	10	$^{16}O + {}^{16}O^{18}O \rightarrow {}^{16}O^{16}O^{18}O$	1.45
	11	$\rightarrow {}^{16}O^{18}O^{16}O$	1.08
	12	$^{18}O + {}^{16}O^{16}O \rightarrow {}^{18}O^{16}O^{16}O$	0.92
	13	$\rightarrow {}^{16}O^{18}O^{16}O$	0.006
51	14	$^{17}O + {}^{17}O^{17}O \rightarrow {}^{17}O^{17}O^{17}O$	1.02
	15	$^{16}O + {}^{17}O^{18}O \rightarrow {}^{16}O^{17}O^{18}O$	
	16	$\rightarrow {}^{16}O^{18}O^{17}O$	
	17	$\rightarrow {}^{17}O^{16}O^{18}O$	
	18	$^{17}O + {}^{16}O^{18}O \rightarrow {}^{17}O^{16}O^{18}O$	
	19	$\rightarrow {}^{17}O^{18}O^{16}O$	
	20	$\rightarrow {}^{16}O^{17}O^{18}O$	
	21	$^{18}O + {}^{16}O^{17}O \rightarrow {}^{18}O^{16}O^{17}O$	
	22	$\rightarrow {}^{18}O^{17}O^{16}O$	
	23	$\rightarrow {}^{16}O^{18}O^{17}O$	
52	24	$^{16}O + {}^{18}O^{18}O \rightarrow {}^{16}O^{18}O^{18}O$	1.50
	25	$\rightarrow {}^{18}O^{16}O^{18}O$	0.029
	26	$^{18}O + {}^{16}O^{18}O \rightarrow {}^{18}O^{16}O^{18}O$	1.04
	27	$\rightarrow {}^{18}O^{18}O^{16}O$	0.92
	28	$^{17}O + {}^{17}O^{18}O \rightarrow {}^{17}O^{17}O^{18}O$	
	29	$\rightarrow {}^{17}O^{18}O^{17}O$	
	30	$^{18}O + {}^{17}O^{17}O \rightarrow {}^{18}O^{17}O^{17}O$	1.03
	31	$\rightarrow {}^{17}O^{18}O^{17}O$	
53	32	$^{17}O + {}^{18}O^{18}O \rightarrow {}^{17}O^{18}O^{18}O$	1.31
	33	$\rightarrow {}^{18}O^{17}O^{18}O$	
	34	$^{18}O + {}^{17}O^{18}O \rightarrow {}^{18}O^{17}O^{18}O$	
	35	$\rightarrow {}^{18}O^{18}O^{17}O$	
54	36	$^{18}O + {}^{18}O^{18}O \rightarrow {}^{18}O^{18}O^{18}O$	1.03

This theory considers (i) an "η-effect", which can be interpreted as a small deviation from the statistical density of states for symmetric isotopomers, compared with the asymmetric isotopomers, (ii) weak collisions for deactivation of the vibrationally excited ozone molecule, and (iii) a partitioning effect ("Y -effect") which controls the recombination rate constant ratios. It arises from small differences in zero point energies of the two exit channels of dissociation of an asymmetric ozone isotopomer, which are magnified into large differences in numbers of states in the two competing exit channel transition state. The considerations (i) and (iii) can be regarded as "symmetry driven" isotope effect. The above-mentioned points are briefly discussed below.

1.3.3.1 Non-Statistical η-Effect

As a modification of classical RRKM theory, it is argued that the effective ρ_{EJ} in Eqn.1.11 might be less than the statistical value and more so for the symmetric isotopomers XYX* than for XYZ*. This ρ_{EJ} should only be the density of the quantum states of the triatomic molecule that are sufficiently dynamically coupled to the two exit channels so that they can lead to the dissociation of the molecule in its typical life-time. After the formation of the vibrationally excited molecule, the subsequent redistribution of the energy among its vibrational-rotational modes at the given *E* and *J* proceeds at some finite rate and may be incomplete during the typical lifetime of the molecule (the non-RRKM effect). The ρ_{EJ} of Eqn.1.11 should only refer to the quantum states, which have been intra-molecularly equilibrated. As there are fewer dynamical coupling terms in the symmetric XYX than in the asymmetric XYZ, some terms being forbidden by the symmetry, it was suggested that this non-RRKM effect for ρ_{EJ} is expected to be greater for XYX than for XYZ. The consequence of this non-statistical effect leads to the non-mass dependent isotopic fractionation.

The above situation is shown pictorially in Figure 1.4. During the typical lifetime of the dissociating ozone, the shaded regions indicate the ozone quantum states sufficiently strongly coupled dynamically to the exit channels so as to contribute to ρ_{EJ} during that lifetime. The shaded region for the asymmetric molecules is shown as a greater fraction of the total region than that of symmetric molecule since there are fewer dynamical coupling terms in the symmetric than in the asymmetric molecule. The ratio of

the fraction of shaded to total region for the asymmetric molecule to the same fraction for the symmetric molecule is denoted by η.

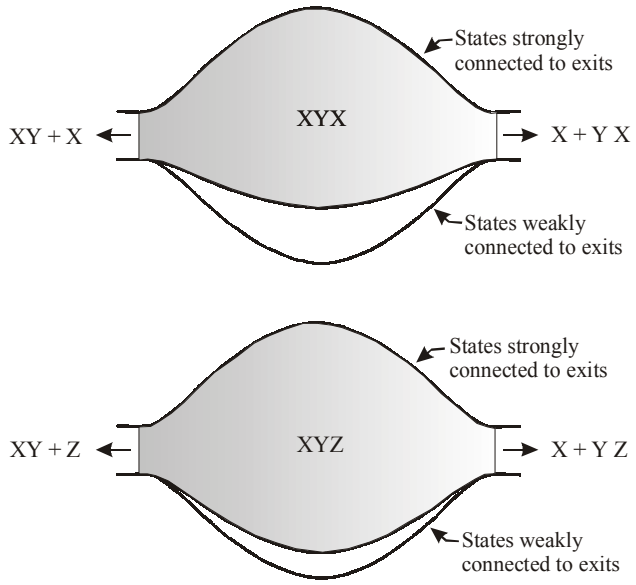

Figure 1.4. *Schematic diagram for XYX and XYZ of differences in ratios of rotational-vibrational states of ozone strongly coupled (shaded region) to the two dissociation exit channels of ozone and those that weakly coupled (unshaded region) to the exit channels [reproduced from Gao and Marcus, 2001].*

1.3.3.2 Weak Collisions for Deactivation

During the stabilization of vibrationally hot molecule (XYZ^*), energy is transferred between excited ozone molecule and a bath gas molecule. The weak collision model assumes that the average energy lost by the vibrationally hot molecule (XYZ^*) in downward collisions and the energy gain in the upward collisions is relatively small. For simplicity, a step-ladder model, in which energy is transferred in discrete steps of ΔE per collision was considered.

1.3.3.3 Partitioning Effect in Dissociation Channels

The reaction scheme of ozone formation includes a redissociation step consisting of two channels, (a) $XYZ^* \rightarrow X + YZ$, and (b) $XYZ^* \rightarrow XY + Z$ when $Z \neq X$. Due to the difference in zero point energy of the product diatomic molecule, the rate constants of these two channels are different and hence, the net bimolecular rate constant of the reaction $X + YZ \rightarrow XYZ$, is dependent on the dissociation channel it follows. So, the dissociation fate of XYZ^* is partitioned into two dissociation channels due to the zero

point energy effect. This partitioning effect is denoted by "Y" ($Y_a = N_{EJ}^{a+}/(N_{EJ}^{a+} + N_{EJ}^{b+})$ and $Y_b = N_{EJ}^{b+}/(N_{EJ}^{a+} + N_{EJ}^{b+})$) in this model.

1.3.4 Interlink Between RRMK Based Theory and Rate Constants

With this non-statistical approach, Gao and Marcus (2001) tried to explain the results of different laboratory experiments (Thiemens and Jackson, 1990; Morton et al, 1990; Anderson et al., 1997; Mauersberger et al., 1999; Janssen et al., 1999). They observed that each model parameter ($\eta, Y, \Delta E$) influences the calculated result of different experiments to different extent, i.e., the calculated results of different experiments are sensitive to different model parameters (see Table 1 of Gao and Marcus, 2001).

The calculated low-pressure rate constants at 300 K of individual channels for the formation of XYZ molecules (using η= 1.18 and ΔE = 210 cm^{-1}) agree well with that of the experimental values (Janssen et al., 1999). The computed isotopic enrichment at low pressure for "scrambled" systems, using these individual rate constants, also agrees with the experimental data of Mauersberger et al. (1999).

In view of the experimental and theoretical studies, the observed anomalous isotopic fractionation in ozone can be explained by sum of the effects arising out of different rate constants of different ozone forming channels. We note that the Gao-Marcus model is restricted to the formation of ozone and does not directly apply to photo-dissociation of ozone. However, the basic idea of departure from a statistical distribution of states can be useful in interpretation of photo-dissociation results.

1.4 ISOTOPIC MEASUREMENTS OF STRATOSPHERIC OZONE

Two types of techniques have been employed for ozone isotopic measurements in the stratosphere: the mass-spectrometric method (*in-situ* and return sample measurement) and the spectroscopic method. The first *in-situ* stratospheric ozone isotopic measurements were performed by Mauersberger (1981). He showed that stratospheric ozone is enriched in ^{18}O ($^{50}O_3 \equiv {}^{16}O^{18}O^{16}O$ and $^{16}O^{16}O^{18}O$) relative to the ambient oxygen from which it is formed. The enrichment is not constant all through the altitude, but shows a peak at around 32 km (with a relative enrichment of 400 ‰). In a later work Mauersberger (1987) showed that the enrichment is not constant, but also varies with the sampling latitude. In

the same study he also showed that for a few altitudes $^{49}O_3$ is also enriched (with large uncertainty) similar to that of $^{50}O_3$.

Schueler et al. (1990) measured the isotopic composition of stratospheric ozone (of collected samples) and found that the enrichment was in the range of 120-160 ‰ for $^{50}O_3$ and 90-110 ‰ for $^{49}O_3$. The nature of the isotopic enrichment was thus found to be mass independent.

Recently Krankowsky et al. (2000) measured the O_3 isotopic composition of a large number of stratospheric samples collected by five different balloon flights during 1998 - 2000 up to an altitude of around 33 km. The maximum enrichment observed was about 110 ‰ at an altitude of 33 km in $^{50}O_3$ and none of the samples showed very high level of enrichment (~ 400 ‰) observed by Mauersberger (1981). The observed enrichment in $^{49}O_3$ (~ 95 ‰) is less than that of $^{50}O_3$ (Mauersberger et al., 2001).

1.4.1 Spectroscopic (Optical) Measurements

Parallel to the mass-spectrometric measurements of stratospheric ozone samples, some workers (Rinsland et al., 1985; Abbas et al., 1987; Goldman et al., 1989; Meier and Notholt, 1996; Irion et al, 1996) have carried out both space and ground based spectral analysis of ozone isotopomers.

Based on spectroscopic parameters derived from laboratory spectra of ozone, Rinsland et al. (1985) determined the heavy ozone content of the total column of ozone from the measurements of three high-resolution solar absorption spectra. Their results indicate only statistically marginally significant enrichments in the column abundances of the heavy isotopomers, by a factor of 1.05 ± 0.07 for $^{16}O^{18}O^{16}O$ and by 1.11 ± 0.11 for $^{16}O^{16}O^{18}O$. Goldman et al. (1989) performed a similar kind of analysis of infrared solar absorption spectra with higher resolution and obtained the column-averaged isotopic enrichment ratio of 1.20 ± 0.14 and 1.40 ± 0.18 for $^{16}O^{18}O^{16}O$ / $^{16}O^{16}O^{16}O$ and $^{16}O^{16}O^{18}O$ / $^{16}O^{16}O^{16}O$ respectively.

Abbas et al. (1987) obtained the distribution of stratospheric heavy ozone isotopomers by balloon based high-resolution thermal emission spectra on the far infrared. The ratio of total heavy ozone isotopomers $^{50}O_3$ to normal $^{48}O_3$ show an enrichment of 450 ‰ at 37 km, decreasing to a minimum of 130 ‰ at ~ 29 km and increasing to 180 ‰ at 25 km.

The vertical enrichment profiles of stratospheric $^{16}O^{16}O^{18}O$ and $^{16}O^{18}O^{16}O$ have been derived from space based ATMOS (Atmospheric Trace Molecule Spectroscopy) FTIR spectrometer by Irion et al. (1996). They have found a column average enrichment of $^{50}O_3$ of (130 ± 50) ‰ with insignificant altitudinal variation.

1.5 SCOPE OF THE PRESENT THESIS

The present thesis investigates the phenomenon of mass independent fractionation in a series of laboratory experiments involving ozone and its interaction with other oxygen containing molecules like CO_2.

The investigation of pressure dependency of oxygen isotopic enrichment in ozone is presented in **Chapter II**. **Chapter III** deals with the experiments on dissociation of ozone by photolysis (in Hartley and Chappuis band) and surface interaction. The laboratory experiments for the investigation of isotopic exchange between ozone photolysis product $O(^1D)$ and CO_2 are described in **Chapter IV**. Implication of some of these laboratory results towards understanding of oxygen isotopic composition in stratospheric ozone and other oxygen containing molecules along with a discussion of major areas of future research are presented in **Chapter V**.